



# OPEN Influence of experimental variables on spheroid attributes

Songshan Zhu<sup>1,2,4</sup>, Jun Yin<sup>3,4</sup>, Xiaotong Lu<sup>1,2,4</sup>, Dan Jiang<sup>1,2</sup>, Rui Chen<sup>1,2</sup>, Kai Cui<sup>1,2</sup>, Wanjun He<sup>1,2</sup>, Na Huang<sup>1,2</sup> & Guangxian Xu<sup>1,2</sup>✉

The adoption of three-dimensional (3D) cell culture systems represents a critical advancement in biomedical research, better mimicking complex 3D tissue environments than traditional two-dimensional (2D) models. However, variability in experimental outcomes has limited their reproducibility and clinical translation. Here, we systematically analyzed 32,000 spheroid images to identify key parameters influencing 3D model reliability. Our large-scale analysis revealed that oxygen levels significantly affect spheroid size and necrosis, while media composition (e.g., glucose and calcium concentrations) and serum levels (0–20%) critically regulate cell viability and structural integrity. For instance, spheroids cultured in 3% oxygen exhibited reduced dimensions and increased necrosis, whereas serum concentrations above 10% promoted dense spheroid formation with distinct necrotic and proliferative zones. By integrating single-cell RNA sequencing and automated image analysis, we uncovered dynamic gene expression patterns linked to spheroid maturation and hypoxia. These findings provide actionable guidelines for standardizing 3D culture protocols, addressing critical reproducibility challenges. Our work establishes a robust framework to enhance the reliability of 3D models in drug testing, personalized medicine, and tumor biology, facilitating their broader adoption in translational research.

**Keywords** 2D cell culture systems, 3D cell culture systems, Experimental conditions, Reproducibility, Standardization

Conventional two-dimensional (2D) monolayer cultures, while instrumental in foundational cell biology research, fail to recapitulate critical *in vivo* microenvironment features such as spatial architecture, biochemical gradients, and cell-ECM interactions<sup>1</sup>. These limitations compromise clinical translatability, exemplified by > 10-fold discrepancies in IC50 values for chemotherapeutics (e.g., doxorubicin) between 2D models and patient-derived 3D tumor systems<sup>2</sup>. Such discordance contributes to the > 90% failure rate of oncology drugs in clinical trials despite promising 2D preclinical data<sup>3</sup>.

Three-dimensional (3D) culture systems, such as spheroids, address these gaps by modeling tissue-specific features like nutrient gradients, zonation (e.g., necrotic core and proliferative periphery), and multicellular crosstalk<sup>4,5</sup>. These models have demonstrated superior predictive power in drug screening; for example, For instance, 3D glioblastoma spheroids replicate patient-derived temozolomide resistance mechanisms<sup>6,7</sup>, demonstrating superior predictive power over 2D counterparts. However, widespread adoption of 3D systems remains hindered by protocol variability—particularly in media composition (e.g., glucose, calcium), oxygen tension, and operator-dependent methods—leading to inconsistent spheroid morphology and behavior<sup>8</sup>.

Emerging technologies like machine learning (ML) and automated image analysis (e.g., AnaSP<sup>9</sup>) offer solutions by enabling real-time quantification of spheroid metrics and predictive toxicity modeling<sup>10–12</sup>. To systematically address reproducibility challenges, we analyzed 32,000 spheroid images to identify critical parameters (oxygen levels, serum concentration, media formulation) influencing 3D model reliability (Fig. 1). Our findings provide actionable guidelines for standardizing 3D culture protocols, enhancing their utility in drug testing, personalized medicine, and tumor biology.

<sup>1</sup>Guangdong Provincial Key Laboratory of Medical Immunology and Molecular Diagnostics, The First Dongguan Affiliated Hospital, School of Medical Technology, Guangdong Medical University, Dongguan, People's Republic of China. <sup>2</sup>Dongguan Key Laboratory of Molecular Immunology and Cell Therapy, Guangdong Medical University, Dongguan, People's Republic of China. <sup>3</sup>Institute of transplantation medicine, The Second Affiliated Hospital of Guangxi Medical University; Guangxi Clinical Research Center for Organ Transplantation; Guangxi Key Laboratory of Organ Donation and Transplantation, Nanning, People's Republic of China. <sup>4</sup>These authors contributed equally: Songshan Zhu, Jun Yin, Xiaotong Lu. ✉email: xuguangxian@gdmu.edu.cn

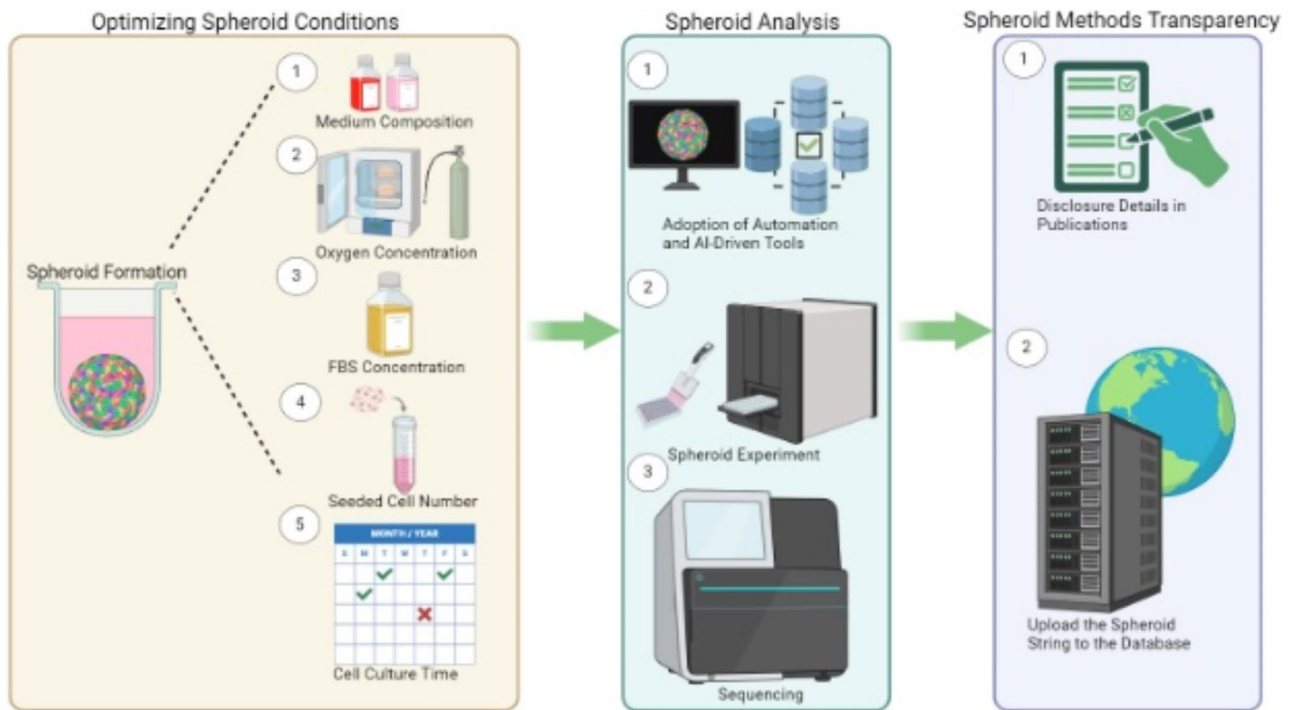


**Fig. 1.** Standardizing 3D spheroid culture: key experimental factors and analysis framework. Standardizing 3D spheroid culture requires optimizing key parameters such as medium composition, oxygen concentration, and FBS levels to ensure consistent formation and growth. Advanced spheroid analysis, including AI-driven tools and automated screening, enhances characterization and reproducibility. Transparent reporting and open-access databases further improve data sharing, facilitating translational applications in drug screening and regenerative medicine. Created with BioRender.com by Songshan Zhu.

## Results

### Impact of culture time on spheroid landscape

MCF-7 spheroids cultured over 19 days exhibited progressive morphological changes. Advanced image analysis was used to monitor spheroid morphology and the dynamic fluorescence of eGFP and PI over time. Key kinetic parameters of spheroid progression at each time point are presented (Fig. 2C and Supplementary Fig. 1A–C). As time progresses, there is a discernible augmentation in the size of spheroids, concomitant with a corresponding diminution in their internal structural integrity and vitality (Fig. 2B,D,E,F, and Supplementary Fig. 1C, D). Correlation analysis further elucidated the disparities in the kinetic parameters of the spheres at different time points (Fig. 2G).

Single-cell RNA sequencing identified two distinct MCF-7 subpopulations with differentiation-stage-specific gene expression (Fig. 2A,H). In 6-day spheroids, upregulated mitochondrial genes were more prevalent in the secondary cell population, whereas in 19-day spheroids, they were primarily enriched in the main cell population. Notably, on day 19, spheroids exhibited high expression of ECM-related genes, including COL18A1, MUC5B, and PIEZO1 (Fig. 2I and Supplementary Fig. 2A–D). Subsequently, we delved into the biological roles of these genes, revealing significant temporal variations in spheroid gene enrichment, including cellular components, molecular functions, and biological pathways, among others (Supplementary Fig. 3B). Remarkably, only 28 genes exhibit identical expression between the two gene profiles, highlighting the novelty of our findings (Fig. 2J). Furthermore, the datasets on gene-gene interactions exhibit substantial divergence, underscoring their role in activating distinct pathways (Supplementary Fig. 3A).

### Insights of impact on spheroid from the different culture mediums

We analyzed commonly available culture media, categorizing their main components into amino acids, inorganic ions, vitamins, and specialized additives (Fig. 3A and Supplementary Fig. 4A–C). This analysis provides insights into media composition and functionality, aiding in cell culture optimization. Notably, media compositions vary significantly and often do not fully replicate plasma. For example, glucose levels are typically 2–5 times higher than in plasma, while calcium levels are often half or lower.

We examined the effects of culture media on HEK 293T spheroid growth kinetics and viability. Growth curves revealed significant differences across media, with compactness, feretDiameterMax, perimeter, and sphericity showing the most variation (Fig. 3B). While equivalent diameter, volume, and fluorescence intensity per spheroid area also followed distinct growth trends, their differences were statistically significant but less pronounced. We subsequently thoroughly compared the differences in spheroid parameters at the culture

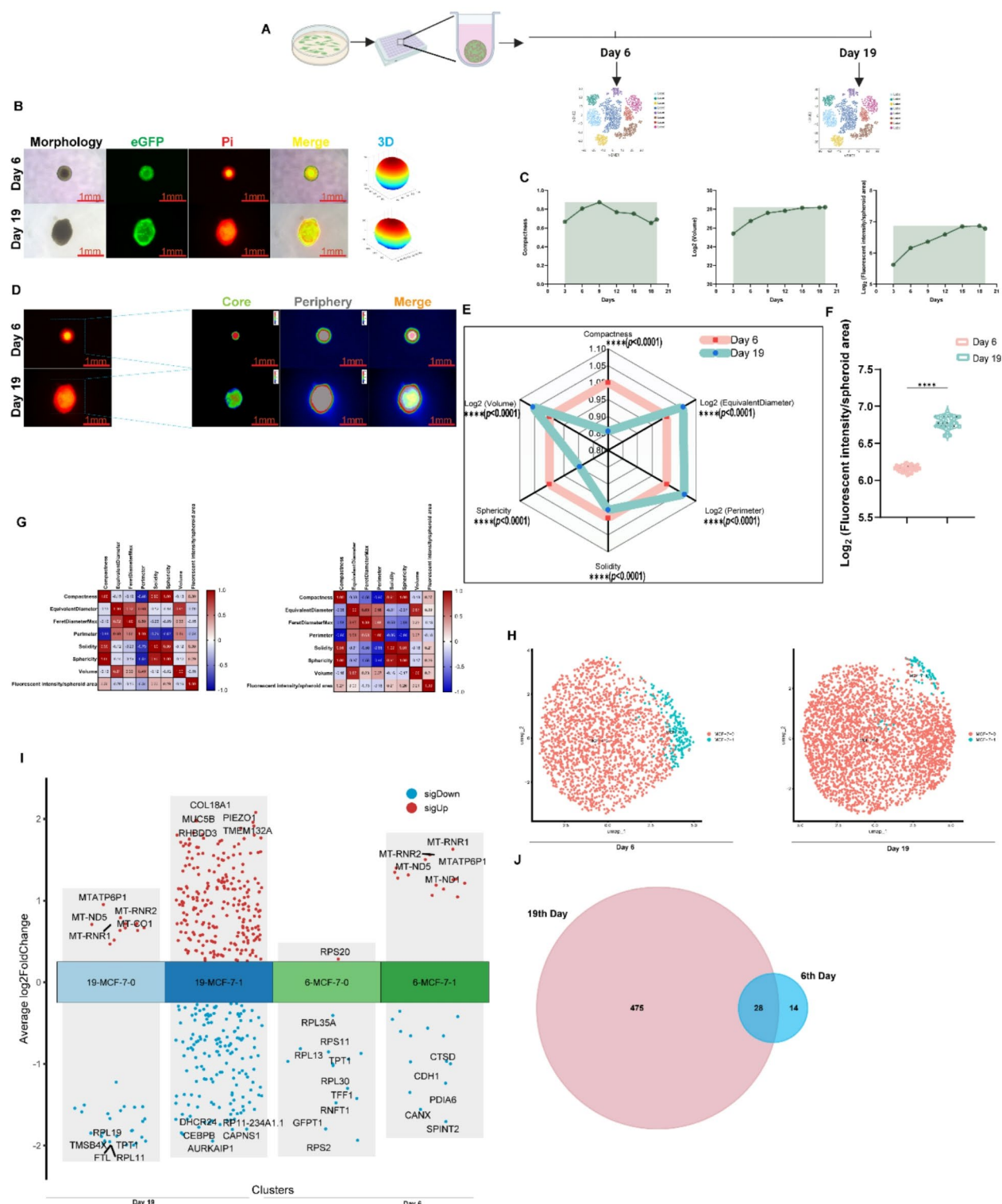


**Fig. 2.** Changes in the MCF-7 spheroid landscape on different days. **(A)** Schematic representation of scRNA-seq analysis of spheroids at different time points. Created with BioRender.com by Songshan Zhu. **(B–F)** Representative images and quantitative analysis of immunofluorescent staining in MCF-7 spheroids at various time points are depicted. Each biological replicate is denoted by a distinct symbol ( $N \geq 3$ ), with each symbol representing a technical replicate ( $n = 12$ ). Scale bar = 1 mm. **(G)** Heatmap illustrating the correlation of sphere parameters is presented. **(H)** The UMAP algorithm applied for dimensionality reduction, successfully classifying two cell clusters. **(I)** Volcano plots displaying gene expression profiles of distinct cell groups within spheroids on days 6 and 19, respectively. **(J)** Venn diagram showing the overlap of differentially expressed genes between subclusters and sample groups of MCF-7 spheroids.

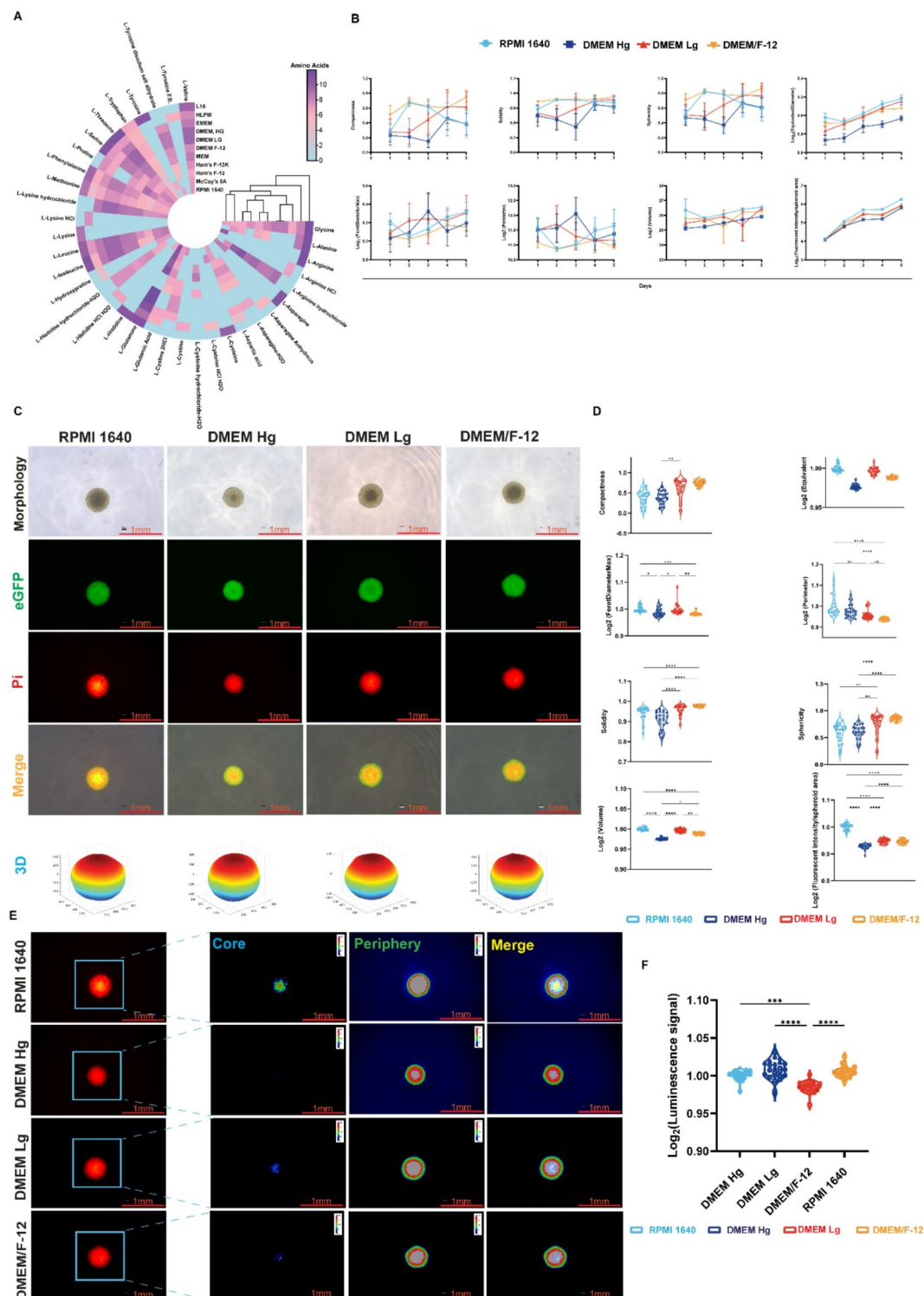


**Fig. 3.** Comparative analysis of HEK 293T spheroid landscapes cultured in various media. (A) Comparative analysis of amino acid content across different culture media. Created with ChiPlot by Songshan Zhu (<https://www.chiplot.online/index.html>). (B) Comparative analysis of amino acid formulations in frequently reported culture media for spheroid research. (C) Image presentation of morphology and cell death in spheroids cultured in different media types. 3D imaging revealed spatial differences in spheroid size and morphology across culture systems. 3D remodeling of spheroids was conducted using ReViSP v2.2 software (<https://sourceforge.net/projects/revisp/>). Scale bar = 1 mm. (D,F) Violin plots illustrating the influence of different culture media on spheroid metrics (D) and ATP content (F) of HEK 293T spheroids. Each biological replicate was denoted by a distinct symbol ( $N \geq 3$ ), with each symbol representing a technical replicate ( $n = 8$ ). (E) Dissecting and comparing fluorescent areas of spheroid death stained with propidium iodide across different culture media. RPMI 1640 increases cell death signals compared to other media, as evidenced by elevated PI fluorescence in necrotic regions. Scale bar = 1 mm.



endpoints. Consistent with the spheroid growth kinetic curves, notable disparities were observed in spheroid size, regularity, death signals, and cell viability (Fig. 3D). Specifically, the fluorescence intensity per spheroid area, indicative of the intensity of the death signal, was significantly elevated under RPMI 1640 culture conditions compared to other culture conditions (Fig. 3C, D). This discrepancy was particularly pronounced in necrotic areas (Fig. 3E). Interestingly, the viability of spheroids was the lowest in DMEM/F12 media (Fig. 3F). A correlation heatmap further highlighted media-dependent parameter relationships. In RPMI 1640 and DMEM Hg, equivalentDiameter correlated strongly with solidity and sphericity, a pattern absent in DMEM Lg and DMEM/F-12 (Supplementary Fig. 4D).

### Serum concentration dictates spheroid architecture

The variability in serum composition used for spheroid establishment prompted us to thoroughly investigate the impact of serum concentration on spheroid characteristics. MCF-7 spheroids displayed Fetal bovine serum (FBS)-dependent growth kinetics (Fig. 4C).

Higher serum concentrations enhance spheroid regularity, density, and size while improving cell viability (Fig. 4A,B,D, and Supplementary Fig. 5A). In serum-free conditions, MCF-7 spheroids shrank over threefold to ~200 µm, with reduced density and increased cell detachment. Spheroids cultured in 10% and 20% serum were the densest, forming distinct necrotic, quiescent, and proliferative zones. Despite these structural differences, spheroid growth remained similar between 10% and 20% FBS (Fig. 4C,D).

Cell death, quantified by fluorescence intensity per spheroid area, was highest in 0.5% and 1% serum but showed no significant difference between 10% and 20% serum (Fig. 4D). ATP content decreased with lower serum concentrations, dropping over 60% below 5% serum, while levels remained stable between 0.5% and 5% (Fig. 4D). Additionally, serum influenced parameter correlations; in serum-free conditions, perimeter showed a strong negative correlation ( $r < -0.9$ ) with compactness, solidity, and sphericity (Fig. 4E).

### The influence of oxygen on the spheroid landscape

Oxygen concentration plays a pivotal role in cell growth dynamics, leading to distinct landscapes within the spheroid microenvironment (Fig. 5A, C,H). Notably, under 3% O<sub>2</sub> conditions, the spheroid exhibits reduced dimensions, including equivalentDiameter and volume. Concurrently, there is a significant decrease in cell viability and ATP content (Fig. 5C), alongside a heightened Pi signal in the necrotic area (Fig. 5B). Interestingly, in co-cultures of Jurkat T cells with spheroids, there appears to be reduced cell death (T cells + cancer cells) under 3% O<sub>2</sub> conditions (Fig. 5D, E). We hypothesize that this hypoxic co-culture microenvironment may favor the survival of Jurkat T cells. In our co-culture experiments, we combined T cells with six spheroid lines derived from different initial seed cell numbers. Notably, we observed a significant decrease in the viability of Jurkat T cells under normal oxygen concentration conditions (Fig. 5F, G).

### The impact of the initial seeded cell number on the spheroid landscape

Spheroid size serves as a crucial parameter for assessing drug penetration and transport within spheroids. The initial choice of seeded cell number profoundly influences spheroid size, thus impacting experimental outcomes. Spheroids established with different initial cell numbers (2000–6000) exhibit cell density-dependent variations in size (Fig. 6A,B,D; Supplementary Fig. 5B,C; Supplementary Fig. 6A,B,D). It's intriguing to note that spheroids formed from distinct cell types display divergent patterns in growth kinetics (Fig. 6C and Supplementary Fig. 6C). As an example, while spheroids derived from MCF-7 cells demonstrate a gradual decrease in size over time, those derived from HCT 116 cells exhibit the opposite trend. Interestingly, when utilizing a seeding cell number of 7000, both spheroid size and cell death were smaller compared to those formed from 6000 cells. Spheroids formed from 6000 cells exhibited the lowest levels of compactness, solidity, and sphericity (Fig. 6D). Surprisingly, when HCT 116 was seeded at higher cell numbers, such as 6000–7000, some spheroids exhibited structural instability. These spheroids ruptured, releasing areas of necrosis and proliferation outside the spheroids (Supplementary Fig. 6A). We also observed a similar phenomenon in MCF-7 cells after 8 days of culture (Supplementary Fig. 5D, E). Interestingly, after 6 days, the spheroid exhibited self-repair capabilities, with its structure returning to normal (Supplementary Fig. 5F). In addition, varying seeding cell numbers can result in substantial differences in the correlations between parameters (Fig. 6E and Supplementary Fig. 6E). For instance, at a seeding cell number of 2000, feretDiameterMax and volume exhibit a strong positive correlation (Fig. 6E).

## Discussion

Spheroid formation occurs in three stages<sup>13</sup>: first, cells aggregate via integrin–ECM interactions; second, cadherin expression increases; and third, homophilic cadherin interactions consolidate a compact structure. Upregulation of cadherin and ECM proteins is crucial. Mature spheroids develop three zones—a necrotic core, a quiescent viable cell region, and an outer proliferative layer—driven by reversed gradients of oxygen, nutrients, and waste. When spheroids exceed 500 µm in diameter, their multilayered architecture restricts the diffusion of essential gases and nutrients while impeding waste removal<sup>4</sup>.

Over time, increasing spheroid size indicates ongoing cellular proliferation and accumulation. The integration of high-throughput image analysis (AnaSP/ReViSP) and scRNA-seq further resolves how these parameters drive transcriptional heterogeneity, providing a molecular basis for protocol optimization. For instance, the discovery of ECM-related gene upregulation (e.g., COL18A1, PIEZO1) under prolonged culture underscores the need to standardize media composition to prevent artefactual matrix deposition. This growth pattern reflects typical spheroid behavior, where proliferating cells aggregate into larger three-dimensional structures. However, the concurrent loss of internal structural integrity and cell vitality raises questions about the underlying mechanisms. It is plausible that as spheroids enlarge, diffusion limitations create hypoxic, nutrient-deprived

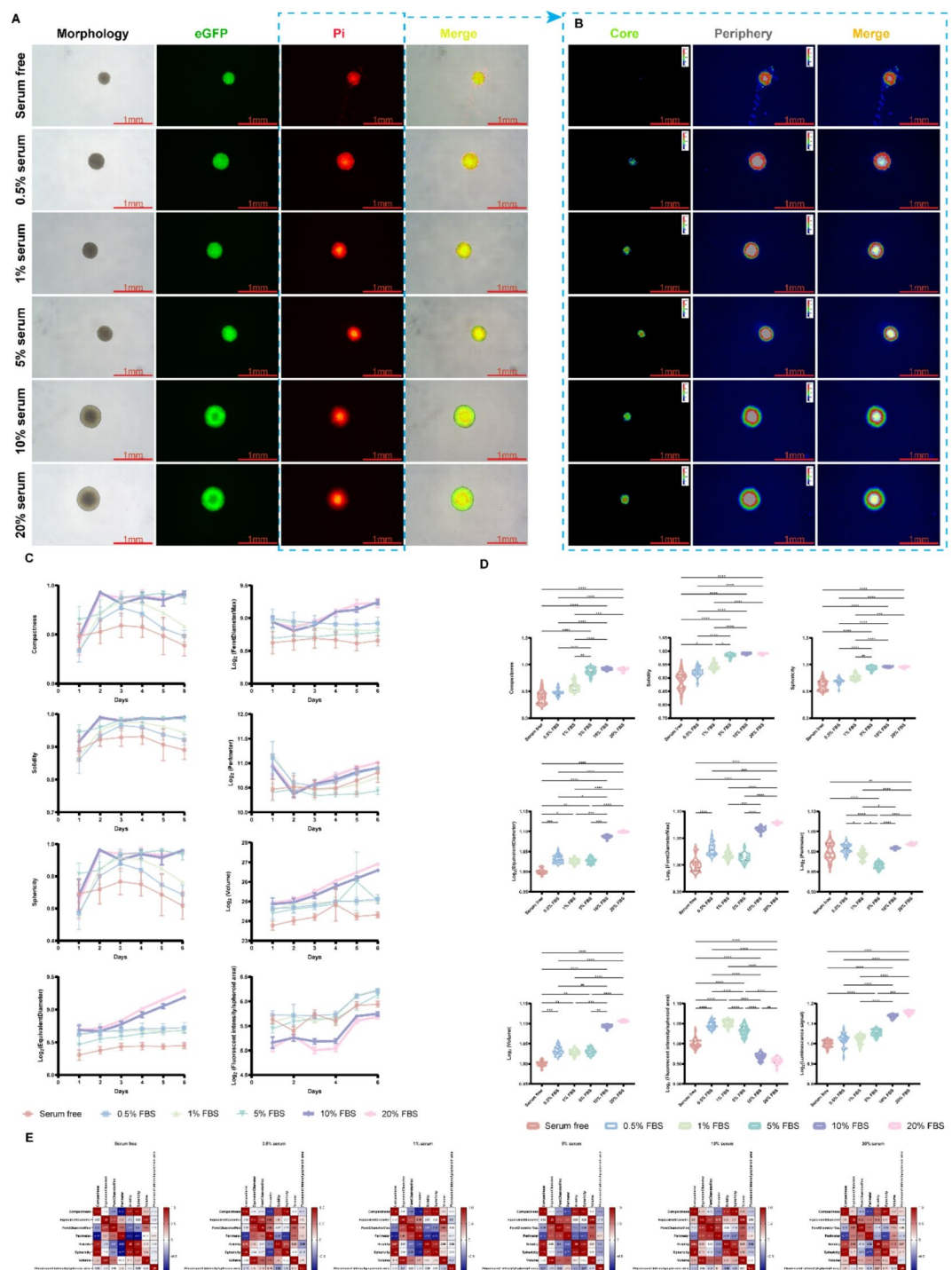


**Fig. 4.** Comparative analysis of spheroid landscapes cultured in various FBS concentration. **(A)** Image presentation of morphology and cell death in spheroids cultured various FBS concentrations. Scale bar = 1 mm. **(B)** Dissecting and comparing fluorescent areas of spheroid death across different culture media. Scale bar = 1 mm. **(C)** Comparative presentation of spheroid growth kinetics across different FBS concentrations. **(D)** Violin plots illustrating the influence of different FBS concentration on spheroid metrics and ATP content of MCF-7 spheroids. Each biological replicate was denoted by a distinct symbol ( $N \geq 3$ ), with each symbol representing a technical replicate ( $n = 8$ ). **(E)** Heatmap illustrating the correlation of MCF-7 spheroid parameters was presented.

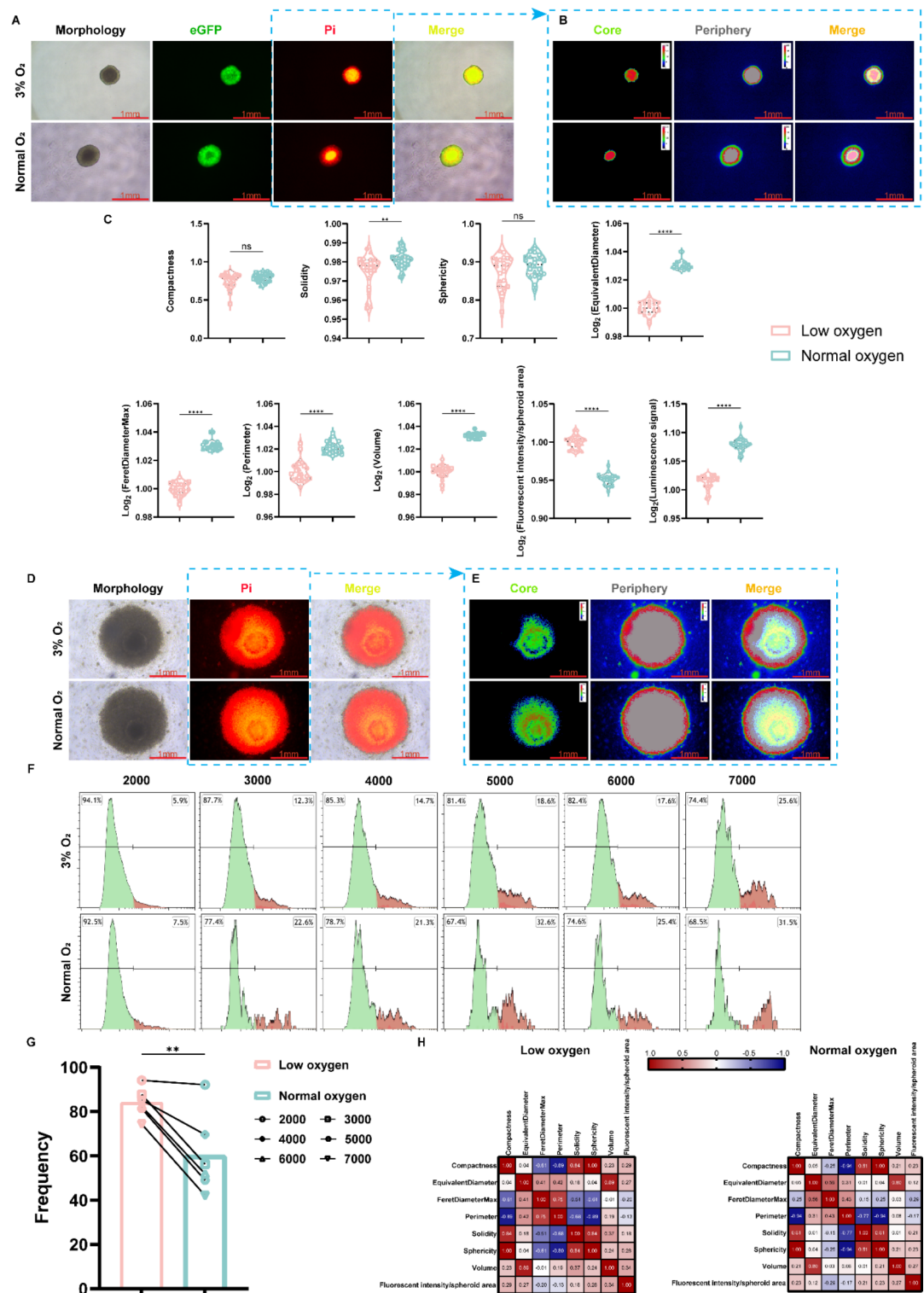
core regions, thereby reducing viability through apoptosis or necrosis. Furthermore, the dynamic fluorescence intensities of eGFP and PI provide additional insights into cellular behavior within the spheroids. A decrease in eGFP fluorescence over time suggests reduced metabolic activity and viability, likely due to hypoxic and nutrient-deprived conditions in the spheroid core. An increase in PI fluorescence indicates progressive necrosis in the inner regions of spheroids as they grow larger. The observed fluorescence changes may reflect shifts in cellular metabolism, viability, and death processes over time. Understanding spheroid evolution is essential for optimizing culture conditions and designing more physiologically relevant models for tumor growth, drug responses, and other biological processes.

The selection of experimental variables in this study, including FBS concentration, oxygen levels, media composition, and initial cell density, were critical for establishing spheroids, yet these factors are often overlooked by researchers. Although culture media are fundamental for supporting cell growth and function, their limitations necessitate alternative strategies to more closely mimic physiological conditions. For example, the amino acid landscape of the lung cancer cell line A549 varies in different microenvironments<sup>14</sup>. Moreover, excessive glucose intake may lead to T cell overactivation and potentially contribute to immune pathology. Tight regulation of glucose uptake is crucial for maintaining immune homeostasis<sup>15</sup>. This underscores the need for the cellular microenvironment to accurately reflect *in vivo* conditions. Additionally, modifying the calcium ion concentration in the culture media may better replicate the *in vivo* environment and enhance the relevance of experimental results, especially in studies focusing on calcium-dependent cellular processes or signaling pathways. Tanaka et al. demonstrated that varying calcium concentrations exert distinct effects on various aspects of osteoblast behavior in 3D culture. Specifically, they found that calcium concentrations influence osteoblast proliferation, survival, differentiation, matrix mineralization, and cytotoxicity<sup>16</sup>. Medium-induced changes in growth kinetics and cell viability in HEK 293T spheroids further highlight the influence of media composition on spheroid development and emphasize the importance of considering multiple parameters when assessing cellular responses in three-dimensional culture systems. In summary, optimizing culture media to better mimic physiological conditions is crucial for ensuring the relevance and reliability of experimental results, particularly in complex biological systems such as spheroid cultures.

FBS concentration is critical in cell culture experiments, as it significantly influences spheroid formation. Spheroid morphology is categorized into three groups based on compactness: compact spheroids, tight aggregates, and loose aggregates of cells<sup>3</sup>. The results show that higher serum levels (10% and 20% FBS) promote the formation of spheroids with greater regularity, density, and size, and with distinct necrotic, quiescent, and proliferative zones. In contrast, lower serum concentrations decrease spheroid density and increase cell detachment, likely due to reduced adhesion-promoting factors. Thus, serum concentration affects not only spheroid size and density but also the spatial distribution of viable and non-viable cells. Interestingly, despite the morphological complexity seen at 10% and 20% FBS, spheroid growth did not significantly differ between these conditions. An FBS concentration of 10–20% provides an optimal balance where serum growth factors (such as IGF, EGF, and TGF- $\beta$ ) promote cell proliferation and adhesion, resulting in effective spheroid formation. Exceeding this range can lead to receptor saturation, negative feedback regulation, and metabolic toxicity, thereby limiting spheroid growth. Conversely, lower serum levels significantly reduce cellular ATP activity by limiting key nutrients like glucose and amino acids, which diminishes glycolysis and mitochondrial oxidative phosphorylation. Nutrient deprivation further triggers autophagy and mitochondrial stress, causing a shift toward less efficient fatty acid oxidation that further depletes ATP levels<sup>17</sup>. Thus, precise optimization of serum concentration is crucial for controlling spheroid formation, growth kinetics, and cellular behavior.

Oxygen profoundly shapes spheroid biology and behavior<sup>18</sup>. Under 3% O<sub>2</sub>, reduced spheroid dimensions underscore the sensitivity of growth to oxygen availability. In subsequent co-culture experiments with non-modified Jurkat T cells—a standard model for T cell signaling—we explored how hypoxia influences immune responses within spheroids. The data suggest that a hypoxic microenvironment modulates cellular interactions, as hypoxia is known to affect immune cell function. For example, TGF- $\beta$  expression synergizes with hypoxia to induce CD8<sup>+</sup> T cell differentiation<sup>19</sup>. Moreover, the hypoxic conditions within the spheroids, by promoting HIF-1 $\alpha$  stabilization and subsequent metabolic reprogramming, not only support tumor cell survival but also lead to the accumulation of immunosuppressive metabolites (e.g., lactate) that may impair T-cell receptor signaling and cytotoxic function. This environment could mimic the *in vivo* tumor microenvironment where hypoxia drives immune evasion through mechanisms such as upregulation of PD-L1 and expansion of regulatory T cells<sup>20</sup>. Thus, understanding oxygen's role is critical for optimizing spheroid culture conditions to faithfully replicate *in vivo* tissue microenvironments, enabling the identification of biomarkers, the development of predictive models, and the design of strategies to promote immune system health and overall physiological well-being<sup>8</sup>.

The initial cell number plays a critical role in determining spheroid size and growth kinetics, which is essential for studies on drug penetration and transport. Spheroids formed from varying cell densities exhibit size differences, underlining the need for controlled seeding. Excessively large spheroids can be fragile and may break during isolation. Moreover, spheroids from different cell types display divergent growth kinetics<sup>6</sup>, reflecting inherent variations in proliferation, metabolism, and intercellular interactions. While a higher initial cell density often produces more compact spheroids with reduced cell death, seeding numbers around 6000–7000 can induce structural instability, leading to spheroid rupture. This instability, termed collective cell movement within the primary tumor, likely results from spatial constraints that drive mesenchymal cells to the periphery, thereby facilitating rapid tumor cell spread and metastasis<sup>21</sup>. Such disruption can confound drug screening results by decreasing viability independent of the therapeutic agent. Interestingly, extending the culture time allows spheroids to self-repair—potentially through the reformation of cell–cell junctions (e.g., via E-cadherin), cytoskeletal reorganization, and activation of survival pathways like PI3K/Akt—which can be verified using time-lapse microscopy, immunostaining, and viability assays. Overall, careful control of initial cell density is crucial for establishing reliable spheroid models in drug testing and related applications.



Efforts to standardize 3D cell culture systems have traditionally focused on spheroid formation and imaging protocols, yet they often overlook scalability and inter-laboratory variability. Variability arises from differences in equipment, reagent sources (e.g., omitted lot numbers), operator expertise, and environmental factors, while fragmented approaches ignore key interactions such as those between serum concentration and oxygen tension<sup>22</sup>. Our study addresses these challenges by offering detailed, transferable protocols and actionable guidelines—including thorough documentation, optimization of variables like serum concentration and cell density, and the use of automated tools—to enhance reproducibility and develop universal metrics for spheroid characterization<sup>10</sup>. We also emphasize inter-laboratory collaboration to validate and refine these standardized protocols.

Our experimental data indicate that media composition, oxygen levels, and FBS concentration critically influence cell metabolism and spheroid formation. For drug screening and metabolic studies, standardizing



**Fig. 5.** Comparative analysis of spheroid landscapes cultured in normal and low oxygen conditions. **(A)** Image presentation of morphology and cell death in MCF-7 spheroids cultured in normal and low oxygen conditions. Scale bar = 1 mm. **(B)** Dissecting and comparing fluorescent areas of spheroid death across different oxygen conditions. Scale bar = 1 mm. **(C)** Violin plots illustrating the influence of different FBS concentration on spheroid metrics and ATP content of MCF-7 spheroids. Each biological replicate was denoted by a distinct symbol ( $N \geq 3$ ), with each symbol representing a technical replicate ( $n = 8$ ). **(D)** Image presentation of morphology and cell death in MCF-7 spheroids following co-culture with Jurkat T cells under normal and low oxygen conditions. Scale bar = 1 mm. **(E)** Dissecting and comparing fluorescent areas of co-culture spheroid death across different culture media. Scale bar = 1 mm. **(F)** Histograms showing frequency of expression in live T cells (green) and dead T cells (red). **(G)** Graph illustrating the average frequency of viable Jurkat T cells at various oxygen concentrations and initial cell numbers seeded into spheroids. **(H)** Heatmap illustrating the correlation of MCF-7 spheroid parameters was presented.

media composition and FBS concentration is essential, whereas tissue engineering requires precise control of physiologically relevant oxygen levels. Comprehensive reporting of culture parameters and standardized operating procedures across labs not only improve reproducibility but also support regulatory approval. The image analysis pipeline faces several limitations, including biases from variations in lighting, uneven fluorescence, and segmentation errors, which we mitigated by validating against manual annotations, and implementing batch processing. Reproducibility challenges also arise due to cell line variability and differences in experimental setups, emphasizing the need for standardized operating procedures across laboratories. Quality control for both imaging and scRNA-seq data was ensured through automated calibration, signal-to-noise monitoring, and robust bioinformatics pipelines with replicate validations. Through detailed investigations of culture media, serum concentration, oxygen availability, and initial cell density, the research provides actionable guidelines for optimizing 3D culture conditions, which can be directly translated into improved drug screening platforms and patient-specific tumor models. Looking forward, the integration of automation and AI-driven quality control measures into the cell culture workflow not only minimizes inter-operator variability but also enhances reproducibility—a factor that is essential for regulatory approval in clinical applications. In this way, our actionable guidelines not only advance fundamental research but also pave the way for the accelerated clinical adoption of 3D culture systems in oncology and regenerative medicine.

## Methods

### Cell culture

Jurkat T, HCT 116 cell lines were purchased from ATCC. HEK 293T cell line was a kind gift from Dr. Yuli Xie. MCF-7 cell line was a kind gift from Dr. Junting He. eGFP-expressing cell lines were stably transduced with the GV513 vector lentiviral. All cell lines undergo rigorous verification through Short Tandem Repeat (STR) Profile testing, ensuring their authenticity and genetic stability. Additionally, routine monthly assessments are conducted utilizing Polymerase Chain Reaction (PCR) to meticulously screen for mycoplasma contamination, thus safeguarding the integrity of experimental outcomes. Jurkat T cells were cultured in RPMI 1640 supplemented with 10% FBS (cat. no. 10091148, GIBCO), 1% penicillin and 1% streptomycin (cat. no. C100C5, NCM). HCT 116, MCF-7, and HEK 293T cells were cultured in DMEM High glucose supplemented with 10% FBS, 1% penicillin and 1% streptomycin. Cells were expanded and maintained as a monolayer at 37 °C in an atmosphere of 5% CO<sub>2</sub> in air and passaged at 70–80% confluence.

### Spheroid formation

The U-shaped, 96-well ultra-low attachment (ULA) plates (cat. no. MS-9096UZ, Sbio) were seeded with a suspension of 180 µl of cell culture media. 2 µg/mL PI (cat. no. 25535164, SIGMA-ALDRICH) was added to the cell suspension to track the cell viability. The culture media used was DMEM LG. All conditions were conducted with 8 (or 12) technical replicates and 3 biological replicates. Cells were cultured at 37 °C in an atmosphere of 5% CO<sub>2</sub> under normoxia.

For comparison of the day point condition,  $2 \times 10^3$  cells (MCF-7-eGFP) were seeded in 180 µl of cell culture medium per well. Photographs of the spheroids were taken every 3 days, and the medium was replaced every 6 days by discarding 90 µl of the old culture medium and adding 90 µl of fresh culture medium, until the 19th day.

Media formulations deviated markedly from physiological plasma to model specific pathophysiological contexts. For example, high glucose (4.5 g/L) in DMEM mimics tumor-associated hyperglycemia, which promotes Warburg metabolism and spheroid expansion, albeit at the cost of increased oxidative stress. Conversely, low calcium in RPMI 1640 disrupts cadherin-mediated cell adhesion, leading to looser spheroid structures. While such deviations reduce direct in vivo relevance, they enable targeted studies of metabolic or adhesive pathways in disease models. For comparison of the culture media condition,  $3 \times 10^3$  cells (HEK 293T-eGFP) were seeded in 180 µl of cell culture medium per well. Photographs of the spheroids were taken daily until the 5th day. Subsequently, the ATP assay was conducted. The culture media used were DMEM HG (cat. no. 10566016, GIBCO), DMEM LG (cat. no. 11885084, GIBCO), DMEM/F12 (cat. no. 11330032, GIBCO), RPMI 1640 (cat. no. 11875093, GIBCO). Most standard culture media contain glucose levels much higher than physiological conditions, leading to altered cell behavior. By systematically evaluating different glucose concentrations, we aimed to understand how metabolic discrepancies affect spheroid formation and reproducibility.

Hypoxia plays a crucial role in tumor microenvironments, influencing gene expression, proliferation, and resistance to therapy. We examined spheroid formation under normoxic (21% O<sub>2</sub>) and hypoxic (3% O<sub>2</sub>) conditions to replicate physiological oxygen gradients and determine their impact on spheroid architecture, viability, and

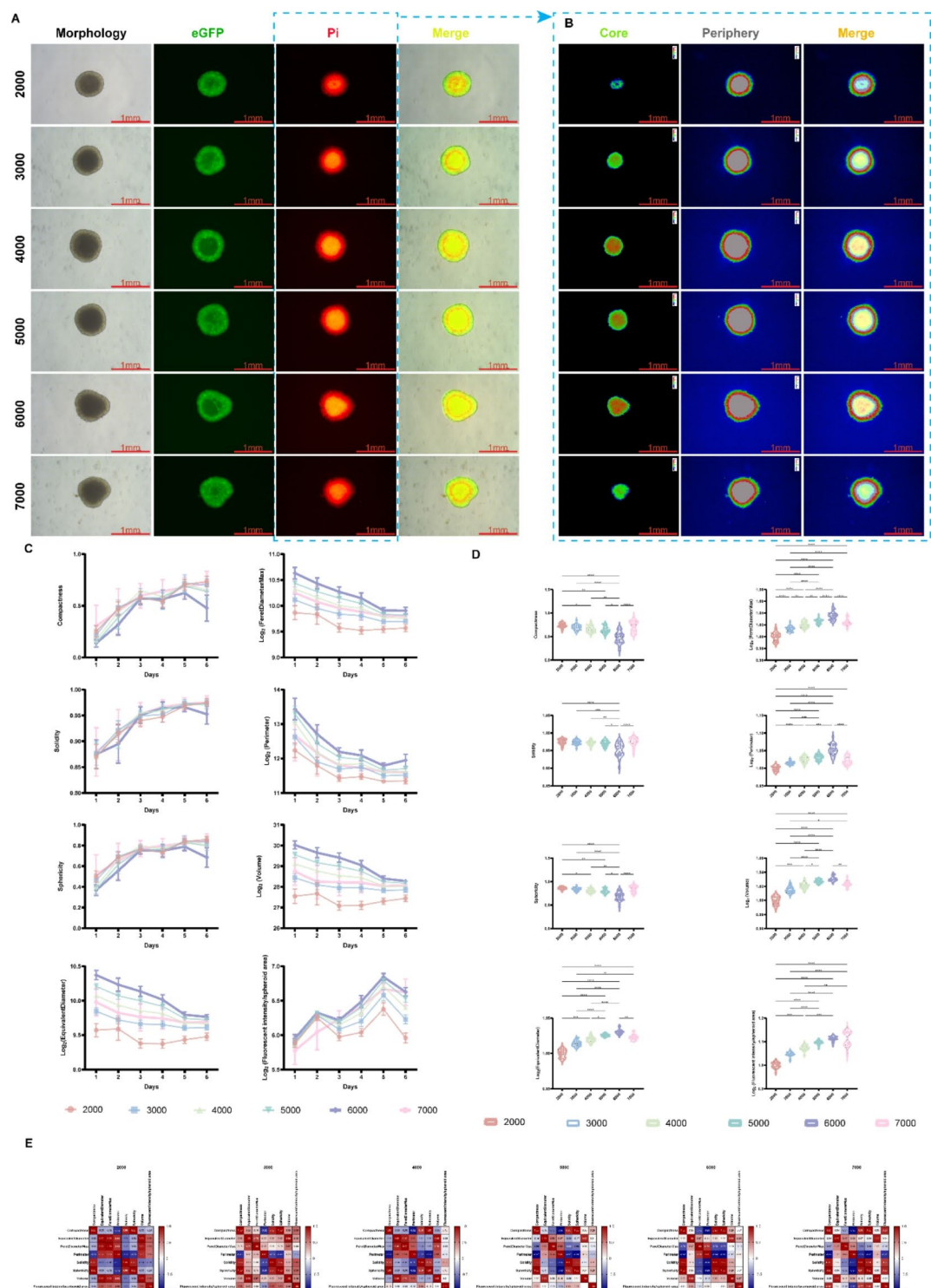


**Fig. 6.** Comparative analysis of MCF-7 spheroid landscapes with varying initial seeded numbers. **(A)** Image presentation of morphology and cell death in spheroids seeded with different cell numbers. Scale bar = 1 mm. **(B)** Dissecting and comparing fluorescent areas of spheroid death across different initial seeded cell numbers. Scale bar = 1 mm. **(C)** Comparative presentation of spheroid growth kinetics across different initial seeded cell numbers. **(D)** Violin plots illustrating the influence of different initial seeded cell numbers on spheroid metrics and ATP content of MCF-7 spheroids. Each biological replicate was denoted by a distinct symbol ( $N \geq 3$ ), with each symbol representing a technical replicate ( $n = 12$ ). **(E)** Heatmap illustrating the correlation of spheroid parameters was presented.

functional zones (necrotic, quiescent, and proliferative regions). For comparison of the normal and low oxygen conditions,  $2 \times 10^3$  cells (MCF-7-eGFP) were seeded in 180  $\mu$ l of cell culture medium per well. The spheroids were cultured for 6 days, and photographs were taken prior to conducting the ATP assay on the final day. For the low oxygen conditions, the atmosphere of 3%  $O_2$  was chosen. Cell seeding was conducted with varying densities:  $2 \times 10^3$ ,  $3 \times 10^3$ ,  $4 \times 10^3$ ,  $5 \times 10^3$ ,  $6 \times 10^3$ , and  $7 \times 10^3$  cells in 180  $\mu$ l of cell culture medium. Culturing conditions encompassed both normal oxygen levels and hypoxic conditions. Following 5 days of culture,  $1.28 \times 10^5$  Jurkat T cells were introduced. After an additional 3 days of culture, the spheroids were dissociated as per the previously outlined method and analyzed using flow cytometry<sup>23</sup>. Briefly, to obtain single cells from spheroids, incubate the spheroids with 0.25% trypsin/EDTA (cat. no. 25200056, GIBCO) at 37 °C for 6–10 min (duration dependent on the size of the spheroids). Flick the tube every 3–5 minutes during the incubation period.

FBS provides essential growth factors, but its undefined composition introduces variability in 3D culture outcomes. For the comparison of FBS conditions, a range of FBS concentrations was selected, comprising serum-free, 0.5% FBS, 1% FBS, 5% FBS, 10% FBS, and 20% FBS. The spheroids were cultured for 6 days, and photographs were taken prior to conducting the ATP assay on the final day.

For the comparison of the seeded cell number conditions, cell seeding was conducted with varying densities:  $2 \times 10^3$ ,  $3 \times 10^3$ ,  $4 \times 10^3$ ,  $5 \times 10^3$ ,  $6 \times 10^3$ , and  $7 \times 10^3$  cells (comprising HCT 116 and MCF-7) in 180  $\mu$ l of cell culture medium.

### Flow cytometry analysis

Single cells were prepared from the co-culture spheroid model following the previously outlined method. Subsequently, cells were harvested by centrifugation and washed twice with PBS. Next, the cells were stained with cell surface marker CD3-APC (cat. no. 3362144, BD) in the dark at 4 °C. Following staining, 450  $\mu$ l of PBS was added, and the samples were analyzed using a Agilent/NovoCyt D3000 flow cytometer. The acquired data were then analyzed using Kaluza software v2.3.0.20268.

### Spheroid image analysis

Segmentation and data extraction of 32,000 spheroid images were conducted using AnaSP v2.1 software<sup>9</sup>. Spheroid metrics, including compactness, equivalent diameter, Feret diameter (maximum), perimeter, solidity, sphericity, and volume, were quantified. Additionally, 3D images of the spheroids were reconstructed using ReViSP v2.2 software, providing a comprehensive visualization of spheroid structure and morphology. For more details on image processing and feature extraction, such as algorithms, please refer to the introduction of AnaSP<sup>9</sup> and ReViSP<sup>24,25</sup>. Spheroid dead fluorescent areas were dissected and compared using ImageJ 1.54 f. These analyses likely contributed to a thorough understanding of spheroid characteristics and facilitated insightful interpretation of experimental results.

### GEO dataset acquisition and analysis

The scRNA-seq raw data of GEO datasets GSE145633 from the Gene Expression Omnibus database (GEO; [www.ncbi.nlm.nih.gov/geo/](http://www.ncbi.nlm.nih.gov/geo/)) were downloaded and analysed. The Seurat package in R version 4.2.2 was used for quality control, statistical analysis, and exploration of the scRNA-seq data. The analysis of gene enrichment, gene interaction, and gene ID conversion was conducted using FunRich 3.1.3 software.

### Cell death staining

The fluorescence signal was monitored either daily or every 3 days at a room temperature of 23 °C using a Nikon/ECLIPSE TS2-f1 fluorescence microscope, equipped with CapStudio Biology 3.8.19 software. The average signal of dead cells was quantified across the spheroid area using Fiji (ImageJ 1.57f). Analysis was conducted on a minimum of three biological replicates, each consisting of a minimum of eight technical replicates per condition. Statistical significance between groups was assessed using a one-way ANOVA followed by Tukey's multiple comparison test, with a significance level ( $\alpha$ ) set at 0.05.

### ATP assay

The spheroids cell viability was detected as the previously outlined method and analyzed using CellTiter-Glo<sup>®</sup> 3D Cell Viability Assay<sup>26</sup>. Briefly, spheroids were cultured in 96-well ultra-low attachment (ULA) plates. Individual spheroids suspended in culture medium were transferred into white 96-well plates (cat. no. 236108, ThermoFisher), followed by the addition of an equal volume of CellTiter-Glo 3D reagent (cat. no. G9683, Promega). The contents were mixed for 5 min on an orbital shaker to induce cell lysis, while shielded from light. After incubation for 25 min at 23 °C (room temperature), luminescence readings were performed using a BioTek SYNERGY H1 microplate reader with Gen5 CHS 3.11 software. Analysis was conducted on a minimum of three biological replicates, each comprising a minimum of eight technical replicates per condition. Statistical significance between groups was assessed using a one-way ANOVA followed by Tukey's multiple comparison test, with a significance level ( $\alpha$ ) set at 0.05.

### Statistical analysis

The data processing procedure commenced with manual exclusion of data points susceptible to interference, such as those affected by dust particles during sphere measurements. Subsequently, outliers were identified and removed using GraphPad Prism v10.1.2 software. This step ensured the integrity and reliability of the dataset, enabling robust statistical analysis and accurate interpretation of results. Statistical analysis was carried out using GraphPad Prism v10.1.2 software. Unpaired comparisons were executed employing either a one-way ANOVA or Kruskal-Wallis test, following the application of mentioned transformations and the Shapiro-Wilk assessment for normality. Subsequently, Tukey's or Dunn's multiple comparison tests were applied, as appropriate.

Comparisons pertaining to the spheroid formation method were conducted using unpaired Student's t-test with Welch's correction. Correlation analysis was performed by determining Pearson or non-parametric Spearman correlation coefficients. The significance level for all tests was set at 0.05. The radar chart for spheroid comparison was generated using OriginPro 2021b software.

## Data availability

The datasets generated and/or analysed during the current study are not publicly available due the data also forms part of an ongoing study but are available from the corresponding author on reasonable request.

Received: 8 November 2024; Accepted: 25 February 2025

Published online: 21 March 2025

## References

- Pampaloni, F., Reynaud, E. G. & Stelzer, E. H. The third dimension bridges the gap between cell culture and live tissue. *Nat. Rev. Mol. Cell. Biol.* **8**, 839–845. <https://doi.org/10.1038/nrm2236> (2007).
- Riedl, A. et al. Comparison of cancer cells in 2D vs 3D culture reveals differences in AKT-mTOR-S6K signaling and drug responses. *J. Cell. Sci.* **130**, 203–218. <https://doi.org/10.1242/jcs.188102> (2017).
- Han, S. J., Kwon, S. & Kim, K. S. Challenges of applying multicellular tumor spheroids in preclinical phase. *Cancer Cell. Int.* **21**, 152. <https://doi.org/10.1186/s12935-021-01853-8> (2021).
- Kunz-Schughart, L. A., Kreutz, M. & Knuechel, R. Multicellular spheroids: a three-dimensional in vitro culture system to study tumour biology. *Int. J. Exp. Pathol.* **79**, 1–23. <https://doi.org/10.1046/j.1365-2613.1998.00051.x> (1998).
- Sumbalova Koledova, Z. In *3D Cell Culture: Methods and Protocols* 1–12 (Springer, 2024).
- Maritan, S. M., Lian, E. Y. & Mulligan, L. M. An efficient and flexible cell aggregation method for 3D spheroid production. *J. Vis. Exp.* <https://doi.org/10.3791/55544> (2017).
- Langhans, S. A. Using 3D in vitro cell culture models in anti-cancer drug discovery. *Expert Opin. Drug Discov.* **16**, 841–850 (2021).
- Chandrasekar, V. et al. Integrated approaches for immunotoxicity risk assessment: challenges and future directions. *Discover Toxicol.* **1**, 9 (2024).
- Piccinini, F. AnaSP: a software suite for automatic image analysis of multicellular spheroids. *Comput. Methods Programs Biomed.* **119**, 43–52. <https://doi.org/10.1016/j.cmpb.2015.02.006> (2015).
- Singh, A. V. et al. AI and ML-based risk assessment of chemicals: predicting carcinogenic risk from chemical-induced genomic instability. *Front. Toxicol.* **6**, 1461587 (2024).
- Chandrasekar, V., Mohammad, S., Aboumarzouk, O., Singh, A. V. & Dakua, S. P. Quantitative prediction of toxicological points of departure using Two-Stage machine learning models: A new approach methodology (NAM) for chemical risk assessment. *J. Hazard. Mater.* **137071** (2025).
- Singh, A. V. et al. Emerging technologies for in vitro inhalation toxicology. *Adv. Healthc. Mater.* **10**, 2100633 (2021).
- Lin, R. Z. & Chang, H. Y. Recent advances in three-dimensional multicellular spheroid culture for biomedical research. *Biotechnol. J.* **3**, 1172–1184. <https://doi.org/10.1002/biot.200700228> (2008).
- Singh, A. V. et al. ToF-SIMS 3D imaging unveils important insights on the cellular microenvironment during biomineralization of gold nanostructures. *Sci. Rep.* **10**, 261. <https://doi.org/10.1038/s41598-019-57136-w> (2020).
- Maciver, N. J. et al. Glucose metabolism in lymphocytes is a regulated process with significant effects on immune cell function and survival. *J. Leukoc. Biol.* **84**, 949–957. <https://doi.org/10.1189/jlb.0108024> (2008).
- Maeno, S. et al. The effect of calcium ion concentration on osteoblast viability, proliferation and differentiation in monolayer and 3D culture. *Biomaterials* **26**, 4847–4855. <https://doi.org/10.1016/j.biomaterials.2005.01.006> (2005).
- Singh, A. V. et al. Evaluating particle emissions and toxicity of 3D pen printed filaments with metal nanoparticles as additives: in vitro and in Silico discriminant function analysis. *ACS Sustain. Chem. Eng.* **9**, 11724–11737 (2021).
- Luo, Z. et al. Hypoxia signaling in human health and diseases: implications and prospects for therapeutics. *Signal. Transduct. Target. Ther.* **7**, 218. <https://doi.org/10.1038/s41392-022-01080-1> (2022).
- Hasan, F., Chiu, Y., Shaw, R. M., Wang, J. & Yee, C. Hypoxia acts as an environmental cue for the human tissue-resident memory T cell differentiation program. *JCI Insight.* **6** <https://doi.org/10.1172/jci.insight.138970> (2021).
- Noman, M. Z. et al. Hypoxia: a key player in antitumor immune response. A review in the theme: cellular responses to hypoxia. *Am. J. Physiology-Cell Physiol.* **309**, C569–C579 (2015).
- Cai, G. et al. Matrix confinement modulates 3D spheroid sorting and burst-like collective migration. *Acta Biomater.* **179**, 192–206. <https://doi.org/10.1016/j.actbio.2024.03.007> (2024).
- Taylor, C. F. et al. Promoting coherent minimum reporting guidelines for biological and biomedical investigations: the MIBBI project. *Nat. Biotechnol.* **26**, 889–896. <https://doi.org/10.1038/nbt.1411> (2008).
- Guo, L., Zhou, Y., Wang, S. & Wu, Y. Epigenetic changes of mesenchymal stem cells in three-dimensional (3D) spheroids. *J. Cell. Mol. Med.* **18**, 2009–2019. <https://doi.org/10.1111/jcmm.12336> (2014).
- Piccinini, F., Tesei, A., Arienti, C. & Bevilacqua, A. Cancer multicellular spheroids: volume assessment from a single 2D projection. *Comput. Methods Programs Biomed.* **118**, 95–106. <https://doi.org/10.1016/j.cmpb.2014.12.003> (2015).
- Piccinini, F., Tesei, A. & Bevilacqua, A. Single-image based methods used for non-invasive volume Estimation of cancer spheroids: a practical assessing approach based on entry-level equipment. *Comput. Methods Programs Biomed.* **135**, 51–60. <https://doi.org/10.1016/j.cmpb.2016.07.024> (2016).
- Peirsman, A. et al. MISpheroID: a knowledgebase and transparency tool for minimum information in spheroid identity. *Nat. Methods.* **18**, 1294–1303. <https://doi.org/10.1038/s41592-021-01291-4> (2021).

## Acknowledgements

GuangDong Basic and Applied Basic Research Foundation (2023A1515140148). High-level Talent Research Funding Program of the First Dongguan Affiliated Hospital of Guangdong Medical University (GCC2023004). Discipline Construction Project of Guangdong Medical University(2051K20220006). Doctoral Initial Funding of Guangdong Medical University(4SG23190G, GDMU2022030). Dongguan Social Development Science and Technology Project (20231800940642).

## Author contributions

The research conceptualization made by S.S.Z., J.Y., and G.X.X. , and methodology and validation made by S.S.Z., X.T.L., D.J., R.C., K.C., W.J.H., and N. H., and formal analysis made by S.S.Z., X.T.L., J.Y., and G.X.X., and writing –Original draft made by S.S.Z., J.Y., and G.X.X.,and visualization made by S.S.Z., J.Y., and writing –



review and editing made by all authors, and project administration made by G.X.X., funding acquisition made by G.X.X.

## Declarations

## Competing interests

The authors declare no competing interests.

## Additional information

**Supplementary Information** The online version contains supplementary material available at <https://doi.org/10.1038/s41598-025-92037-1>.

**Correspondence** and requests for materials should be addressed to G.X.

**Reprints and permissions information** is available at [www.nature.com/reprints](http://www.nature.com/reprints).

**Publisher's note** Springer Nature remains neutral with regard to jurisdictional claims in published maps and institutional affiliations.

**Open Access** This article is licensed under a Creative Commons Attribution-NonCommercial-NoDerivatives 4.0 International License, which permits any non-commercial use, sharing, distribution and reproduction in any medium or format, as long as you give appropriate credit to the original author(s) and the source, provide a link to the Creative Commons licence, and indicate if you modified the licensed material. You do not have permission under this licence to share adapted material derived from this article or parts of it. The images or other third party material in this article are included in the article's Creative Commons licence, unless indicated otherwise in a credit line to the material. If material is not included in the article's Creative Commons licence and your intended use is not permitted by statutory regulation or exceeds the permitted use, you will need to obtain permission directly from the copyright holder. To view a copy of this licence, visit <http://creativecommons.org/licenses/by-nc-nd/4.0/>.

© The Author(s) 2025